applied sciences

MDPI

Article

Controllable Fano-like Resonance in Terahertz Planar Meta-Rotamers

Subin Jo, Min-Gyu Bae and Joong-Wook Lee *

Department of Physics and Optoelectronics Convergence Research Center, Chonnam National University, Gwangju 61186, Korea; whtnqls1995@gmail.com (S.J.); baemingyu357@gmail.com (M.-G.B.)
* Correspondence: leejujc@chonnam.ac.kr

Abstract: Meta-molecules composed of meta-atoms exhibit various electromagnetic phenomena owing to the interaction among the resonance modes of the meta-atoms. In this study, we numerically investigated Fano-like-resonant planar metamaterials composed of meta-molecules at terahertz (THz) frequencies. We present meta-rotamers based only on the difference in the spatial position of their component meta-atoms (C- and Y-shapes) that can be interconverted by rotations and have tunable Fano-like resonance. This is because of the cooperative effects determined by the spatial coupling conditions of the nodes and antinodes of electric-dipole and inductive–capacitive (LC) resonances of the meta-atoms. The findings of this study provide potential options for exploring novel THz devices and for engineering high-level functionalities in metamaterial-based devices.

Keywords: terahertz spectroscopy; metamaterials; modulators; active optics

check for updates

Citation: Jo, S.; Bae, M.-G.; Lee, J.-W. Controllable Fano-like Resonance in Terahertz Planar Meta-Rotamers. *Appl. Sci.* **2021**, *11*, 9796. https://doi.org/10.3390/app11219796

Academic Editor: Mira Naftaly

Received: 22 September 2021
Accepted: 19 October 2021
Published: 20 October 2021

Publisher's Note: MDPI stays neutral with regard to jurisdictional claims in published maps and institutional affiliations.

Copyright: © 2021 by the authors. Licensee MDPI, Basel, Switzerland. This article is an open access article distributed under the terms and conditions of the Creative Commons Attribution (CC BY) license (https://creativecommons.org/licenses/by/4.0/).

1. Introduction

The creation of metamaterials, which are artificially constructed composite materials with exceptional properties, has become an extremely interesting area of research in various fields, such as optics, optoelectronics, electromagnetic field, acoustics, and thermology [1–4]. Artificial atoms (called meta-atoms) or molecules (called meta-molecules), as the basic structural elements for constructing metamaterials, are designed and fabricated to implement a device with the desired characteristics and functionalities. In particular, the meta-molecules created by engineering spatial arrangement or interatomic geometry of different types of meta-atoms achieve high-level functionalities, such as plasmon-induced transparency, multifunctional filtering, invisibility cloaking, tunable multiple resonators, reflective-index engineering, and Fano resonance [5–18].

Recently, metamaterials have promoted the inclusive development of terahertz (THz) materials and devices because of their resonant electromagnetic response, which significantly improves the interaction between THz radiation and metamaterials. In particular, developing THz devices and building a network connection in the THz frequencies have become key tasks for achieving sixth-generation (6G) wireless communication [19,20]. This requires new techniques to manipulate the polarization, direction, amplification, collimation, resonance frequency, propagation, and phase of those THz waves. Thus, a THz metamaterial is the best candidate for realizing a device with such functionalities.

Meta-molecules composed of different types of meta-atoms are fundamental elements that control the transmission, reflection, and absorption of light and realize the tunability of resonance wavelength at the THz frequencies. Various electromagnetically induced transparency (EIT)-analog optical systems based on THz metamaterials exhibit a narrow transmission or reflection spectral band and plasmon-induced transparency behavior [21–24]. The EIT-like effects of bright–bright mode coupling, which occur when two resonances of two different types of meta-atoms are excited in close proximity in the spectral domain, inevitably lead to resonance frequency detuning based on Fano-type interference with ultrahigh quality factor (Q-factor) [25–27]. Therefore, metamaterials

composed of meta-molecules are essential for fabricating versatile THz devices that require the ability to control resonance modes and spectral features.

In this study, we numerically investigated a Fano-like-resonant planar THz metamaterial composed of meta-molecules consisting of two different types of meta-atoms, C- and Y-shaped metallic rods. In addition, we demonstrated that meta-rotamers based only on the difference in the spatial position of their component meta-atoms manifest tunable Fano-like resonance when optically isotropic, inner Y-shaped meta-atoms rotate. This phenomenon is caused by cooperative effects due to the spatial coupling conditions of the nodes and antinodes of the fundamental electric-dipole resonance of Y-shaped meta-atoms and higher-order inductive–capacitive (LC) resonance of C-shaped meta-atoms. Our study highlights the importance of metamaterials for achieving novel THz devices and their high-level functionalities.

2. Design and Methods

Figure 1a shows a representative unit cell of the proposed metamaterial numerically simulated in this study. The two top virtual layers have two different types of meta-atoms, a C-shaped metallic split-ring resonator (SRR) with spatially varying geometric parameters and a Y-shaped metallic rod with different rotation angles. The meta-molecule shown in the lowest layer of Figure 1a can be considered a unit cell of composite metamaterials, produced by combining the SRR and the Y-shaped rod.

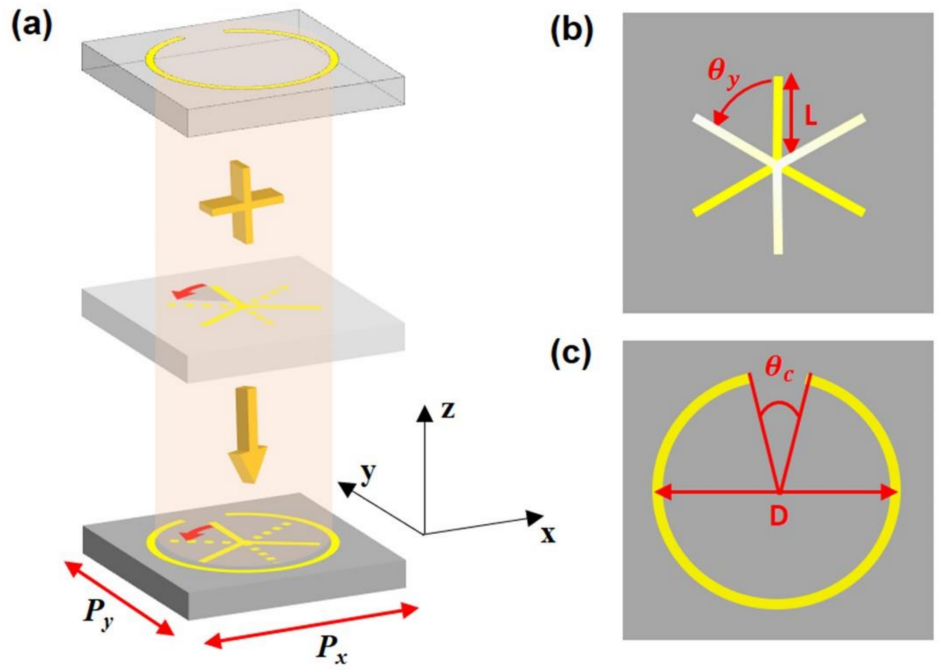


Figure 1. (**a**) Schematic of the THz planar meta-rotamer consisting of the C-shaped SRR and Y-shaped metal rod. The physical dimensions of the meta-molecules in the lattice are $P_x = P_y = 120$ μm. The thicknesses of the meta-molecules and dielectric substrate (bare silicon) are 150 nm and 200 μm, respectively. (**b**) Schematic of the Y-shaped meta-atom. The corresponding size and rotations are as follows: $L = 40$ μm; $\theta_y = 0°$, 30°, and 60°. (**c**) Schematic of the C-shaped SRR meta-atom. The corresponding size and angular gaps are as follows: $D = 100$ μm; $\theta_c = 10°$, 20°, and 30°.

The two types of meta-atoms are structurally combined to be an analog of rotational isomers (also called rotamers) in chemistry, in which the rotamers can be interconverted by rotations. By combining the rotating Y-shaped meta-atoms to the fixed SRR meta-atom, the arrangements of meta-atoms in a meta-molecule that are transformed by rotation about the central axis of bonding can be exploited to generate different conformations that provide a possible method to design promising THz devices.

The basic components (C-shaped SRR and Y-shaped rod) display optimal characteristics for fabricating the composite metamaterials, which can also be called meta-rotamers. The Y-shaped meta-atom is one of the simplest structures showing polarization-insensitive transmission or absorption properties because of its higher-order rotational symmetry and folded-slot resonators; moreover, it is available to fabricate multimode resonators and active control devices [28–33]. As shown in Figure 2a, the folded planar resonator consisting of two arms placed in the direction of polarization of the incident THz waves generates a dipole resonance with a resonant wavelength equal to twice the length of the metal rod [31]. When the Y-shaped meta-atom rotates, the three arms alternately assume the function of the folded planar resonator while exhibiting polarization-independent optical properties, as shown in the inset of Figure 2a. Here, the normalization was carried out by dividing the spectral amplitudes through the metamaterials by the spectral amplitude through bare silicon used as a substrate.

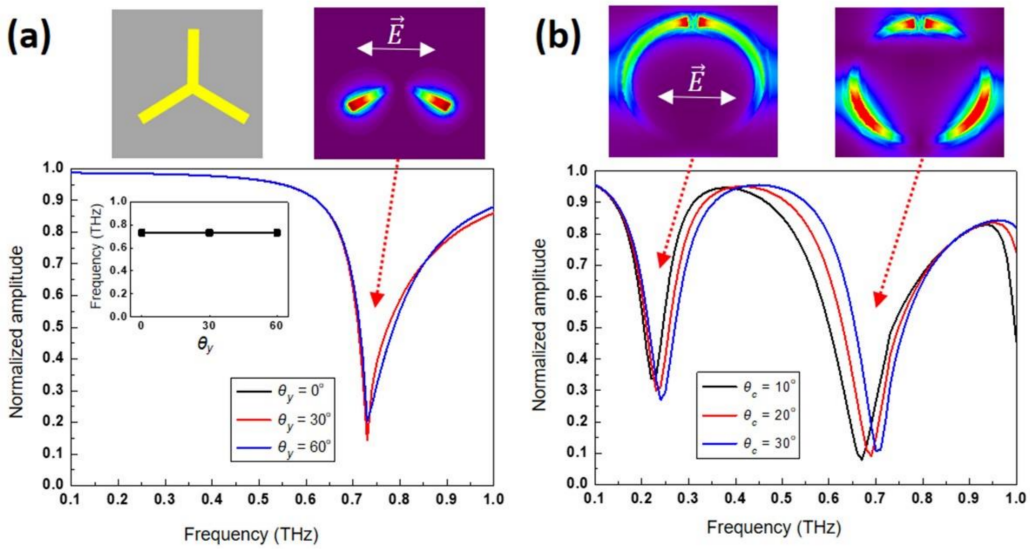


Figure 2. (**a**) Simulated THz amplitude spectra in the arrays of Y-shaped meta-atoms at the rotation angles of θ_y = 0°, 30°, and 60°. The inset shows the values of resonance frequency. The upper image shows the near electric field distribution at the resonance frequency at the rotation angle of θ_y = 0°. (**b**) Simulated THz amplitude spectra in the arrays of C-shaped SRR meta-atoms at the angular gaps of θ_c = 10°, 20°, and 30°. The upper images show the near electric field distributions at the resonances appearing near the frequencies of 0.25 and 0.7 THz.

The C-shaped SRR meta-atom leads to dramatic structure-dependent features. The tunability of optical resonances can be achieved by varying the arc length of the C-shaped, polarization-dependent characteristics due to high structural asymmetry, and the fabrication of composite medium with simultaneously negative values of effective permeability and permittivity. As a result, versatile and novel optical devices can be realized, such as negative refractive index devices, superlenses, multifunctional filters, polarization devices, and various types of resonators [34–38]. Figure 2b shows the simulated THz amplitude spectra in the arrays of C-shaped SRR meta-atoms with angular gaps of θ_c = 10°, 20°, and 30°. As the total arc length of the C-shape is shorter, the two odd resonances are blue-shifted because the resonance wavelength depends on the arc length of the C-shape.

As in the aforementioned case, when the polarization of the incident light at normal incidence is parallel to the gap of the C-shaped SRR, the two odd resonances appearing near the frequencies of 0.25 THz and 0.7 THz can be clearly observed. As can be inferred from the two electric near-field images on the top, one appears at the lower frequency and corresponds to the fundamental LC resonance, whereas the other appears at the higher frequency and corresponds to the second-order LC resonance (also called quadrupole-mode resonance) [25]. The meta-molecules are designed such that the electric-dipole resonance

of the Y-shaped meta-atom can be overlapped on the quadrupole-mode resonance of the C-shaped SRR in frequency.

All simulations were performed using COMSOL Multiphysics software, which is a frequency-domain solver based on the finite element method (FEM), to solve the Maxwell equations. For the structure of the metamaterial unit cell, the unit element was surrounded by periodic boundary conditions on four sides, and the top and bottom of the unit element were considered as perfectly matched layers. The simulated structure was illuminated by an x-polarized plane wave at normal incidence. Most metals can be regarded as perfect conductors at THz frequencies. Therefore, we obtained the values of permittivity, plasma frequency, and damping constant of aluminum required for the simulations using the Drude model [39]. In addition, the silicon layer with a thickness of 200 μm was modeled as a lossless dielectric substrate with a relative permittivity of 11.68.

3. Results and Discussion

Figure 3a demonstrates the simulated amplitude spectra of THz wave transmission for the meta-rotamer displayed in Figure 1a. For the two transition states of the meta-rotamers with different angles of rotation of $\theta_y = 0^\circ$ and 60°, the transmission spectra clearly present two resonant dips corresponding to the frequencies of f_1 and f_2 at $\theta_y = 0^\circ$ and f'_1 and f'_2 at $\theta_y = 60^\circ$. f_1 and f'_1 represent the second-order LC resonance of the C-shaped SRR, whereas f_2 and f'_2 represent the electric-dipole resonance of the Y-shaped rod.

To elucidate the characteristics of the resonances, we simulated the electric near-field distributions at the four resonant frequencies shown in Figure 3a. To clearly observe the spatial shape of each resonance mode, we plotted the out-of-plane electric field (E_z) distributions at the distance of 8 μm above the surface of the meta-rotamers, as shown in Figure 3b. The figures of f_2 and f'_2 show that the dipole resonance mode corresponding to the two arms of the Y-shaped metal rod lying in the polarization direction of the incident THz waves is well represented for both states of the meta-atoms. In this case, only the position of the electric near-field pattern is changed because of the structural change of the meta-molecules, whereas the shape of the electric near-field pattern and the position of the resonant frequency do not change.

On the contrary, in the case of the second-order LC resonance appearing at the frequencies of f_1 and f'_1, a completely different aspect is observed. The resonance mode for the C-shaped meta-atom does not show a clear difference for the two states of meta-rotamers. However, when the angle of rotation is 0° for the Y-shaped rod, the electric near-field is activated at the ends of its arms horizontal to the polarization. When the arms of the Y-shaped rod are adjacent to the standing wave antinodes of the second-order LC resonance, the electric near-fields are strongly enhanced at the ends of its arms. This implies that the coherent near-field coupling between the bright modes of two adjacent meta-atoms occurs when the antinodes of the two excited resonances are located close to each other with a gap of 5 μm.

To generate a stronger coupling effect, the total length of the C-shaped SRR was tuned; thus, the two resonant modes were close to each other in the spectrum. As the angular gap changed from 10° to 30°, the second-order LC resonance f'_1 approached the dipole resonance f'_2 of the Y-shaped rod, as shown by the red curves in Figure 3a,c,e. When the antinode coupling of the two excited resonances at the meta-rotamer state with $\theta_y = 0^\circ$ appeared, the second-order LC resonance f_1 shifted to the longer wavelength regime. Interestingly, the second-order LC resonance changed significantly with an asymmetrical line shape, whereas the dipole resonance was almost unchanged. This implies that, when the standing wave antinodes of the two excited resonances are spatially overlapped, the two resonances strongly interfere with each other, thereby generating Fano-like resonance. It is known that the strong red-shift of f'_1 in the spectral band is caused by the damping phenomenon of localized surface waves, depending on the coupling strength between the two standing wave antinodes [40,41].

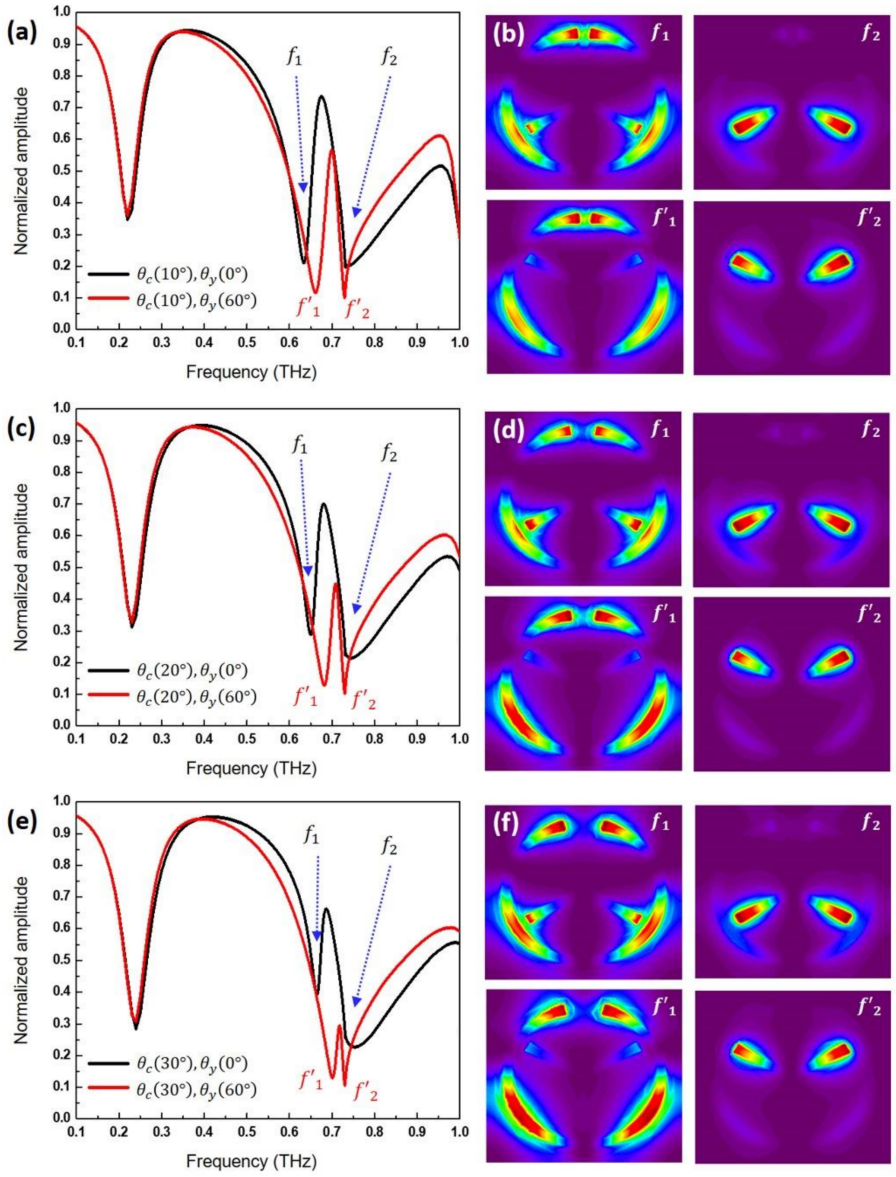


Figure 3. (**a**,**c**,**e**) Simulated THz amplitude spectra in the meta-rotamers consisting of the C-shaped SRR and Y-shaped rod meta-atoms, for the two different states of the meta-rotamers with rotation angles of $\theta_y = 0°$ and 60°, as shown by the black and red solid lines, respectively. Each THz amplitude spectra were simulated in the three types of samples with different angular gaps of θ_c = 10°, 20°, and 30°, as shown in (**a**,**c**,**e**), respectively. (**b**,**d**,**f**) Spatial electric near-field distributions for the meta-molecules at the resonances of f_1, f_2, f'_1 and f'_2. For the three types of samples with different angular gaps of θ_c = 10°, 20°, and 30°, f_1 = 0.63, 0.65, and 0.66 THz, f_2 = 0.74, 0.74, and 0.74 THz, f'_1 = 0.66, 0.68, and 0.70 THz, and f'_2 = 0.73, 0.73, and 0.73 THz, respectively.

To quantitatively understand the dependence of coupling strength on the state of meta-rotamer, we plotted the values of resonant frequency extracted from the simulations versus the angular gap θ_c, for the structure with only C-shaped SRR meta-atoms and the meta-rotamers with two different states, which are determined by different angular gaps, as shown by the black squares, red circles, and blue triangles in Figure 4a, respectively. When the two standing wave antinodes were not aligned, the combined effect of the C- and Y-shaped meta-atoms appeared as a simple summation of each resonance without a significant change in the resonant frequency, as shown by the red circles in Figure 4a. On the contrary, the clear red-shift of the second-order LC resonance was visible because of the strong coupling when the standing wave antinodes were placed opposite to each other,

as quantitatively compared in Figure 4b, which shows the values of resonant frequency shift, $\Delta f_1 = f'_1 - f_1$ and $\Delta f_2 = f'_2 - f_2$.

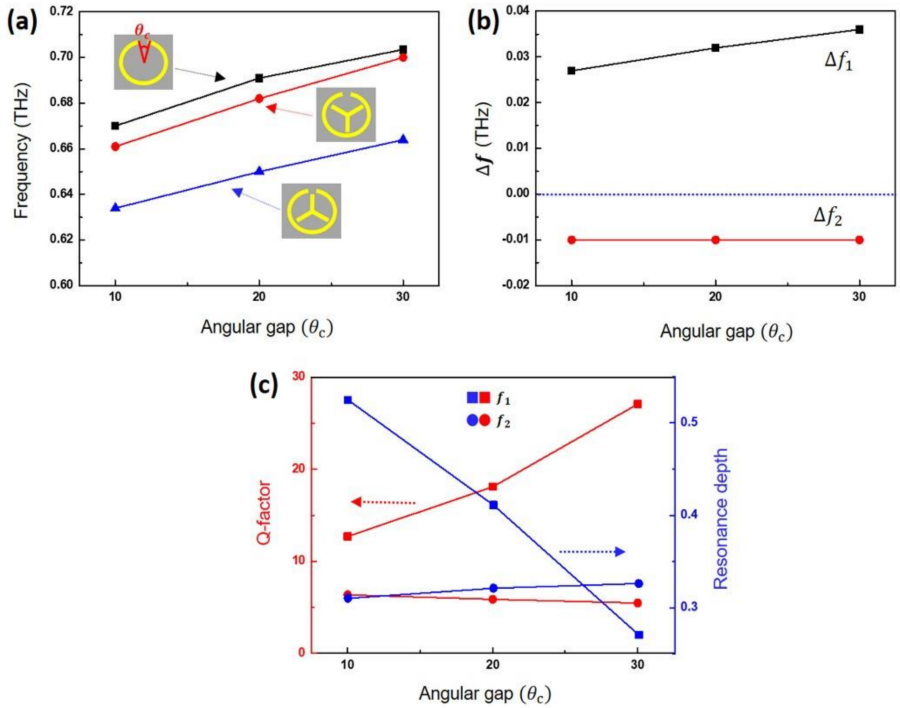


Figure 4. (**a**) Resonant frequencies of the second-order LC resonance obtained at three samples of the C-shaped meta-atoms and two states of meta-rotamers. (**b**) Frequency shift of the second-order LC resonance (Δf_1) and dipole resonance (Δf_2) as a function of angular gap θ_c. (**c**) Q-factor (red squares and circles, left scale) and resonance depth (blue squares and circles, right scale) for the two resonances, f_1 (blue and red squares) and f_2 (red and blue circles), respectively.

The coupling strength is important in achieving resonance characteristics such as a high Q-factor. As shown in Figure 4c, the Q-factor exhibits an interesting growth behavior with the increase of the angular gap showing higher coupling strength between the two resonances. Here, if the coupling strength is increased by approximating the two resonances in the spectrum, a larger Q-factor can be expected. Although we expected to maximize the Q-factor and the resonance strength, there was a tradeoff between these factors, which is a typical characteristic of the resonance phenomenon, as shown in the values of resonance depth (blue squares). On the contrary, the Q-factor and resonance depth extracted from the dipole resonance of the Y-shaped rods exhibited a slight difference by varying the angular gap. Thus, the asymmetric feature of the Fano-like resonance caused by the strong coupling between each resonance of two different types of meta-atoms suggests a method to control the resonant frequency and the Q-factor.

4. Conclusions

In conclusion, we have demonstrated meta-rotamers with Fano-like resonance. The meta-rotamers based only on the difference in the spatial position of their component meta-atoms, the C-shaped SRR and Y-shaped metal rod, can be interconverted by the rotation of the Y-shaped meta-atom. The resonant frequency and the Q-factor can be controlled by asymmetric characteristics of Fano-like resonance. This is because of the cooperative effects determined by the spatial coupling conditions of nodes and antinodes of the second-order LC resonance by the C-shaped SRR meta-atoms and the dipole resonance by the Y-shaped meta-atoms. The higher Q-factor observed in the antinode–antinode combination is due to the strong electric near-field coupling between two resonant modes located spectrally very close together. In addition, the red-shift of the LC resonance may be caused by the

increase of effective inductance value in the condition of the antinode–antinode coupling. We believe that the findings provide possibilities for exploring metamaterial-based THz devices, such as modulators, sensors, antennas, and switches, requiring high sensitivity and multifunctions of spectral tunability and selectivity.

Author Contributions: Conceptualization and methodology, J.-W.L.; writing—original draft preparation, S.J.; writing—review and editing, J.-W.L. and M.-G.B.; data acquisition and analysis, S.J. and M.-G.B.; supervision, project administration, and funding acquisition, J.-W.L. All authors have read and agreed to the published version of the manuscript.

Funding: National Research Foundation of Korea (NRF) grant funded by the Korea government (MSIT) (Grant Number: NRF- 2019R1F1A1058851).

Institutional Review Board Statement: Not applicable.

Informed Consent Statement: Not applicable.

Data Availability Statement: Data are contained within the article.

Conflicts of Interest: The authors declare no conflict of interest.

References

1. Cui, T.J.; Qi, M.Q.; Wan, X.; Zhao, J.; Cheng, Q. Coding metamaterials, digital metamaterials and programmable metamaterials. *Light Sci. Appl.* **2014**, *3*, e218. [CrossRef]
2. Jung, J.; Park, H.; Park, J.; Chang, T.; Shin, J. Broadband metamaterials and metasurfaces: A review from the perspectives of materials and devices. *Nanophotonics* **2020**, *9*, 3165–3196. [CrossRef]
3. Lee, J.-H.; Singer, J.P.; Thomas, E.L. Micro-/nanostructured mechanical metamaterials. *Adv. Mater.* **2012**, *24*, 4782–4810. [CrossRef]
4. Zheludev, N.I.; Kivshar, Y.S. From metamaterials to metadevices. *Nat. Mater.* **2012**, *11*, 917–924. [CrossRef] [PubMed]
5. Lee, I.-S.; Sohn, I.-B.; Kang, C.; Kee, C.-S.; Yang, J.-K.; Lee, J.W. High refractive index metamaterials using corrugated metallic slots. *Opt. Express* **2017**, *25*, 6365–6371. [CrossRef] [PubMed]
6. Lee, J.W.; Seo, M.A.; Park, D.J.; Kim, D.S.; Jeoung, S.C.; Lienau, C.; Park, Q.H.; Planken, P.C.M. Shape resonance omni-directional terahertz filters with near-unity transmittance. *Opt. Express* **2006**, *14*, 1253–1259. [CrossRef] [PubMed]
7. Liu, N.; Langguth, L.; Weiss, T.; Kästel, J.; Fleischhauer, M.; Pfau, T.; Giessen, H. Plasmonic analogue of electromagnetically induced transparency at the Drude damping limit. *Nat. Mater.* **2009**, *8*, 758–762. [CrossRef]
8. Zhang, S.; Genov, D.A.; Wang, Y.; Liu, M.; Zhang, X. Plasmon-induced transparency in metamaterials. *Phys. Rev. Lett.* **2008**, *101*, 047401. [CrossRef]
9. Ziemkiewicz, D.; Słowik, K.; Zielińska-Raczyńska, S. Ultraslow long-living plasmons with electromagnetically induced transparency. *Opt. Lett.* **2018**, *43*, 490–493. [CrossRef]
10. Ling, Y.; Huang, L.; Hong, W.; Liu, T.; Luan, J.; Liu, W.; Lai, J.; Li, H. Polarization-controlled dynamically switchable plasmon-induced transparency in plasmonic metamaterial. *Nanoscale* **2018**, *10*, 19517–19523. [CrossRef]
11. Hentschel, M.; Saliba, M.; Vogelgesang, R.; Giessen, H.; Alivisatos, A.P.; Liu, N. Transition from isolated to collective modes in plasmonic oligomers. *Nano Lett.* **2010**, *10*, 2721–2726. [CrossRef]
12. Papasimakis, N.; Fedotov, V.A.; Zheludev, N.I.; Prosvirnin, S.L. Metamaterial analog of electromagnetically induced transparency. *Phys. Rev. Lett.* **2008**, *101*, 253903. [CrossRef]
13. Schurig, D.; Mock, J.J.; Justice, B.J.; Cummer, S.A.; Pendry, J.B.; Starr, A.F.; Smith, D.R. Metamaterial electromagnetic cloak at microwave frequencies. *Science* **2006**, *314*, 977–980. [CrossRef]
14. Liu, J.-Q.; Yu, J.-M. Electromagnetic resonances and their tunability in planar metamolecules isomer. *Optik* **2015**, *126*, 2858–2861. [CrossRef]
15. Omaghali, N.E.J.; Tkachenko, V.; Andreone, A.; Abbate, G. Optical sensing using dark mode excitation in an asymmetric dimer metamaterial. *Sensors* **2014**, *14*, 272–282. [CrossRef]
16. Yang, Z.-J.; Wang, Q.-Q.; Lin, H.-Q. Cooperative effects of two optical dipole antennas coupled to plasmonic Fabry–Pérot cavity. *Nanoscale* **2012**, *4*, 5308–5311. [CrossRef]
17. Liu, N.; Weiss, T.; Mesch, M.; Langguth, L.; Eigenthaler, U.; Hirscher, M.; Sönnichsen, C.; Giessen, H. Planar metamaterial analogue of electromagnetically induced transparency for plasmonic sensing. *Nano Lett.* **2010**, *10*, 1103–1107. [CrossRef] [PubMed]
18. Liu, N.; Kaiser, S.; Giessen, H. Magnetoinductive and electroinductive coupling in plasmonic metamaterial molecules. *Adv. Mater.* **2008**, *20*, 4521–4525. [CrossRef]
19. Yang, P.; Xiao, Y.; Xiao, M.; Li, S. 6G wireless communications: Vision and potential techniques. *IEEE Netw.* **2019**, *33*, 70–75. [CrossRef]
20. Dang, S.; Amin, O.; Shihada, B.; Alouini, M.-S. What should 6G be? *Nat. Electron.* **2020**, *3*, 20–29. [CrossRef]
21. Singh, R.; Rockstuhl, C.; Lederer, F.; Zhang, W. Coupling between a dark and a bright eigenmode in a terahertz metamaterial. *Phys. Rev. B* **2009**, *79*, 085111. [CrossRef]

22. Liu, M.; Tian, Z.; Zhang, X.; Gu, J.; Ouyang, C.; Han, J.; Zhang, W. Tailoring the plasmon-induced transparency resonances in terahertz metamaterials. *Opt. Express* **2017**, *25*, 19844–19855. [CrossRef]
23. Baqir, M.A.; Choudhury, P.K.; Farmani, A.; Younas, T.; Arshad, J.; Mir, A.; Karimi, S. Tunable plasmon induced transparency in graphene and hyperbolic metamaterial-based structure. *IEEE Photonics J.* **2019**, *11*, 1–10. [CrossRef]
24. Yao, F.; Li, F.; He, Z.; Liu, Y.; Xu, L.; Han, X. Tunable fano resonances in an ultra-small gap. *Appl. Sci.* **2020**, *10*, 2603. [CrossRef]
25. Al-Naib, I.; Yang, Y.; Dignam, M.M.; Zhang, W.; Singh, R. Ultra-high Q even eigenmode resonance in terahertz metamaterials. *Appl. Phys. Lett.* **2015**, *106*, 011102. [CrossRef]
26. Cong, L.; Manjappa, M.; Xu, N.; Al-Naib, I.; Zhang, W.; Singh, R. Fano resonances in terahertz metasurfaces: A figure of merit optimization. *Adv. Opt. Mater.* **2015**, *3*, 1537–1543. [CrossRef]
27. Yan, F.; Li, Q.; Wang, Z.; Tian, H.; Li, L. Extremely high Q-factor terahertz metasurface using reconstructive coherent mode resonance. *Opt. Express* **2021**, *29*, 7015–7023. [CrossRef] [PubMed]
28. Grant, J.; Ma, Y.; Saha, S.; Khalid, A.; Cumming, D.R.S. Polarization insensitive, broadband terahertz metamaterial absorber. *Opt. Lett.* **2011**, *36*, 3476–3478. [CrossRef]
29. Du, C.; Zhou, D.; Guo, H.-H.; Pang, Y.-Q.; Shi, H.-Y.; Liu, W.-F.; Singh, C.; Trukhanov, S.; Trukhanov, A.; Xu, Z. Active control scattering manipulation for realization of switchable EIT-like response metamaterial. *Opt. Commun.* **2021**, *483*, 126664. [CrossRef]
30. Lee, J.-W.; Yang, J.-K.; Sohn, I.-B.; Choi, H.-K.; Kang, C.; Kee, C.-S. Relationship between the order of rotation symmetry in perforated apertures and terahertz transmission characteristics. *Opt. Eng.* **2012**, *51*, 119002. [CrossRef]
31. Lee, J.W.; Yang, J.-K.; Sohn, I.-B.; Kang, C.; Kee, C.-S. Folded slot resonator array with efficient terahertz transmission. *Opt. Commun.* **2013**, *293*, 155–159. [CrossRef]
32. Lee, J.W.; Yang, J.-K.; Sohn, I.-B.; Yoo, H.K.; Kang, C.; Kee, C.-S. Monopole resonators in planar plasmonic metamaterials. *Opt. Express* **2014**, *22*, 18433–18438. [CrossRef] [PubMed]
33. Song, M.-S.; Lee, I.-S.; Sohn, I.-B.; Kang, C.; Kee, C.-S.; Yang, J.-K.; Lee, J.W. Characteristics of multi-mode resonances in T-shape air slots. *AIP Adv.* **2015**, *5*, 047107. [CrossRef]
34. Wang, Z.; Yao, K.; Chen, M.; Chen, H.; Liu, Y. Manipulating Smith–Purcell emission with babinet metasurfaces. *Phys. Rev. Lett.* **2016**, *117*, 157401. [CrossRef] [PubMed]
35. Lapine, M.; Shadrivov, I.V.; Powell, D.A.; Kivshar, Y.S. Magnetoelastic metamaterials. *Nat. Mater.* **2012**, *11*, 30–33. [CrossRef]
36. Lee, J.W.; Seo, M.A.; Kim, D.S.; Kang, J.H.; Park, Q.-H. Polarization dependent transmission through asymmetric C-shaped holes. *Appl. Phys. Lett.* **2009**, *94*, 081102. [CrossRef]
37. Smith, D.R.; Padilla, W.J.; Vier, D.C.; Nemat-Nasser, S.C.; Schultz, S. Composite medium with simultaneously negative permeability and permittivity. *Phys. Rev. Lett.* **2000**, *84*, 4184–4187. [CrossRef] [PubMed]
38. Clark, A.W.; Sheridan, A.K.; Glidle, A.; Cumming, D.R.S.; Cooper, J.M. Tuneable visible resonances in crescent shaped nano-split-ring resonators. *Appl. Phys. Lett.* **2007**, *91*, 093109. [CrossRef]
39. Palik, E.D. (Ed.) *Handbook of Optical Constants of Solids*; Academic Press: Orlando, FL, USA, 1985.
40. Mock, J.J.; Hill, R.T.; Tsai, Y.-J.; Chilkoti, A.; Smith, D.R. Probing dynamically tunable localized surface plasmon resonances of film-coupled nanoparticles by evanescent wave excitation. *Nano Lett.* **2012**, *12*, 1757–1764. [CrossRef] [PubMed]
41. Trivedi, R.; Thomas, A.; Dhawan, A. Full-wave electromagentic analysis of a plasmonic nanoparticle separated from a plasmonic film by a thin spacer layer. *Opt. Express* **2014**, *22*, 19970–19989. [CrossRef]